To cite this version :

Mamoun FELLAH, Mohammed Abdul SAMAD, Mohamed LABAIZ, Omar ASSALA, Alain IOST - Sliding friction and wear performance of the nano-bioceramic -Al 2 O 3 prepared by high energy milling - Tribology International - Vol. 91, p.151-159 - 2015
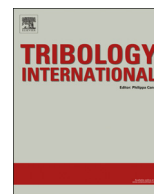
Contents lists available at ScienceDirect

Tribology International

journal homepage: www.elsevier.com/locate/triboint

Sliding friction and wear performance of the nano-bioceramic α-Al$_2$O$_3$ prepared by high energy milling

Mamoun Fellah [a,b,*], Mohammed Abdul Samad [c,1], Mohamed Labaiz [a,2], Omar Assala [a,3], Alain Iost [d,4]

[a] Surface Engineering and Tribology Group, Laboratory of Metallurgy and Engineering Materials, BADJI Mokhtar-Annaba University, P.O. 12, 23000 Algeria
[b] Mechanical Engineering Department, ABBES Laghrour- Khenchela University, P.O 1252, 40004, Algeria
[c] Mechanical Engineering Department, King Fahd University of Petroleum & Minerals. Box 1180, Dhahran 31261, Saudi Arabia
[d] Laboratory of Mechanics Surfaces and processing materials, ARTS ET METIERS ParisTech, 8, Boulevard Louis XIV, 59046 Lille Cedex, France

ARTICLE INFO

ABSTRACT

The structural evolution and morphological changes of the nanostructured α-Al$_2$O$_3$ powder using different milling times (1, 8, 16 and 24 h) were studied. It is observed that the crystallite size of the particles reduced to 2 nm after milling for 24 h. Morphological studies of powder particles indicated that the powder particle size continuously decreases with increasing milling time. The sliding wear rate and wear coefficient of friction were lower in the nanocrystalline samples milled at 24 h at same applied load (3, 6 or 10 N). The improved friction and wear resistance is attributed to the finer microstructure of the sample milled for 24 h.

© 2015 Elsevier Ltd. All rights reserved.

1. Introduction

The problems of friction and wear in the prosthesis for substitution of hip joints and knees have been addressed by many authors [1–6], due to its crucial importance in the performance of these devices. The choice of the materials for the head and the cup takes into consideration not only properties such as mechanical resistance, friction and wear, but also biocompatibility and corrosion resistance. Ceramic components have been used for total hip arthroplasty in Europe since the early 1970s, with good results [7–9]. Such components afford a number of theoretical advantages compared to metal alloys. They have been shown to have excellent biocompatibility both in animal studies and clinical investigations in Europe [10]. Ceramics can be given a very high, scratch-resistant polish. This feature, combined with wettability and corrosion resistance of the material, allows for low friction articulations with excellent wear characteristics [11–13].

Repeated mechanical loadings, due to human gait and micro-separation between head and cup, are imposed on the surface between a head and a cup of artificial hip prosthesis, leading to shock degradations [14,15]. Failure of hip prosthesis resulting from shocks brings about serious damages to the human body. For this reason, shock degradation is one of the critical concerns in the design of hip prosthesis. Several studies were carried out in order to investigate mechanical and wear damages of hip prostheses [16–21].

Nanocrystalline ceramics are being studied extensively by reducing grain sizes with the aim of improving their mechanical properties as well [22–24]. The improvement was in terms of higher hardness [25–26] better crack propagation resistance, i.e. fracture toughness [27–31]. However, there are counterclaims in the literature contradicting these observations [32–38]. Therefore, the benefit of nanocrystallinity of ceramics for improved tribological properties has not been demonstrated unequivocally. Correlations among milling conditions, microstructure, mechanical behavior, and tribological characteristics have not been fully established.

The process of obtaining nanocrystalline feed stock plays a significant role in determining its properties [39,40]. Mechanical milling of initially microcrystalline powders is a quick and an effective method for producing nanocrystalline powders in large quantities, when compared to chemical synthesis routes [41–43]. The melting behavior of mechanically milled nanocrystalline powders is expected to be different from other nanocrystalline powders. Hence, the microstructure and tribological behavior of alumina samples produced from high energy mechanically milled nanocrystalline powders and hot isostatic (HIP) need to be investigated.

* Corresponding author. Tel.: +213 660 34 88 85.
E-mail addresses: mamoun.fellah@yahoo.fr (M. Fellah),
samad@kfupm.edu.sa (M. Abdul Samad), m.labaiz@univ-annaba.org (M. Labaiz),
asslo23@gmail.com (O. Assala), Alain.IOST@ENSAM.EU (A. Iost).
[1] Tel.: +966 13 8601082.
[2] Tel.: +213 778369024.
[3] Tel.: +213 663715288.
[4] Tel.: +333 20622233.

The milling time is one of the most important parameter in mechanical milling is based on their ability to significantly improve the wear resistance and durability of THP [44–46]. Normally the time is so chosen as to achieve a steady state between the fracturing and cold welding of the powder particles. The times required vary depending on the type of mill used, the intensity of milling, the ball-to-powder ratio, and the temperature of milling. These times have to be decided for each combination of the above parameters and for the particular powder system. But, it should be realized that the level of contamination increases and some undesirable phases form if the powder is milled for times longer than required. Therefore, it is desirable that the powder is milled just for the required duration and not any longer [47]. Hence the current research was under taken to study a nanocrystalline α-alumina sample produced by high energy milling followed by uniaxial pressing and HIP treatment to evaluate the friction and wear properties, microstructure, lattice parameters and hardness as a function of milling time and nanocrystallinity.

2. Experimental details

2.1. Materials and synthesis processes

2.1.1. High energy ball milling process

Alumina powder with a purity of 99.97% and an average particle size in the range of 5–30 μm and a density of 3.97 g/cm^3 is used. The powder was milled at different milling times 1, 8, 16, and 24 h, under an argon atmosphere, nominally at room temperature in a high energy planetary ball mill (Fritsch P7) with a rotation speed of 300 rpm. The milling media consisted of twenty 20 mm diameter ball confined in a 300 ml volume vial. The ball-to-powder weight ratio was about 18. The milling was carried out in cycles of 25 min with a 10 min of pause in between. For each milling operation the vials were opened only after a cooling period of 40–55 min.

2.1.2. Hot Isostatic Pressing (HIP) processes

The milled Al$_2$O$_3$ powders were uniaxially pressed at 150 MPa into discs of 17 mm in diameter and 4 mm thickness using a rigid steel die. The compaction was carried out using an *Elvc Hydraulic press* at a constant strain rate. After ejecting from the die, the samples were measured and weighed to calculate the density. Green compacts were placed into an alumina crucible with Al$_2$O$_3$ powder and sintered at temperatures of 1450 °C for 2 h at a heating rate of 30 K min^{-1} in order to obtain a closed porosity (high density) as observed by Bocangera [48]. The sintered samples were then introduced into a boron nitride crucible with an alumina powder bed to minimize possible reactions with the graphite heating element and subsequently hot isostatically pressed in an ASEA-HIP (QIH-6) at 1325 °C and 1350 °C respectively at a heating rate of 30 K min^{-1} and at an isostatic pressure of 150 MPa for 35 min.

The temperature of sintering and hot pressing of the alumina was determined on the basis of the previous published work of many authors [11,35,36]. This HIP treatment was applied to the powder in order to produce a fine grained material with a final relative density of 98%. The density was measured geometrically by immersion using the Archimedes principle.

2.2. Physical and mechanical characterizations

2.2.1. Physical characterization

To characterize the microstructure, the specimens were ground and polished with 0.1 nm diamond paste. After preparing the surfaces by dry grinding and polishing, sintered specimens were thermally etched at 1300 °C for 27 min and characterized by scanning electron microscopy (*SEM: JOEL JSM-35C*) using an accelerating voltage of 2–15 kV, to investigate the particle size and morphology. Samples were carbon coated to avoid charging during exposure to the electron beam. Linear intermission electron microscopy was employed to observe the morphology of the starting powders and measure their average grain size. The structural evolution and the phase identification was characterized by X-ray diffractometry (XRD) with Cu-K$\langle\alpha\rangle$ radiation ($\langle\lambda\rangle$ Cu$=0.15406$ nm) in a ($\langle\theta\rangle$–$\langle2\theta\rangle$) Bragg-Brentano geometry.

2.2.2. Microhardness

The hardness and elastic modulus of bio-ceramic was evaluated from the load-penetration depth curves obtained from a nanoindontation tester (*Zwik ZHV 2.5*) with Berkovich diamond indenter (*B-J87*). The elastic constant $E_i=1141$ GPa and Poisson ration's $\nu_i=0.07$ are often used for diamond indenter. Prior to the nanoindentation tests, the surface of the sample was polished and wiped with alcohol and dried thoroughly. In order to take the repeatability into account, the test results were acquired from the average of four indentations.

2.2.3. Tribological characterizations

Friction and wear tests were conducted using a conventional ball-on-disk type Oscillating tribometer testing machine (*TRIBO-tester*) under dry conditions in ambient air and 6 mm track radius in accordance with the ASTMG 99, ISO 7148, and ASTM G 133-95 standards. The tests were carried out under a wide range of applied loads (3, 6 and 10 N), as shown in Fig. 1 with an alumina ball (Al$_2$O$_3$) for which the young modulus$=310$ GPa, HV$_{0.05}=2400$ and density of 3.97 g/cm^3 as a counterface. α-Al$_2$O$_3$ ceramics, prepared by high energy ball milling followed by HIP at 1350 °C by the process described earlier, were cut into disk specimens for different types of tests and polished to a surface roughness (Ra) of $0.55-0.75$ nm.

Before each test, the specimens and the balls were rinsed ultrasonically in acetone. After the tribological tests, the worn surfaces of the specimens were observed by an optical and scanning electron microscopy (SEM) respectively. Samples and alumina balls were weighed before and after the tests, but not much significant difference in the weight was observed. So the following wear rate equation was applied:

$$W = V/F \cdot L \tag{01}$$

where V is the wear volume (μm^3), F is the applied load (N) and L is the sliding distance (μm). The wear volume was determined by the integration of the worn track profile obtained by laser and mechanical profilometry with

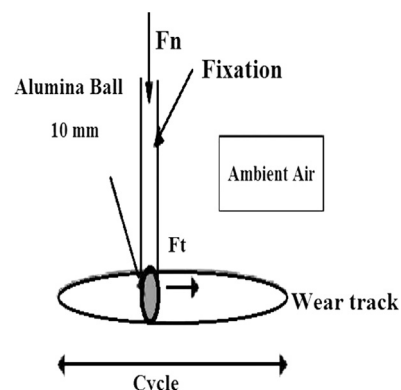$$V = \pi h^2[R-(h/3)] + [R^2\alpha - l(R/2)\cos(\alpha)] \tag{02}$$

Fig. 1. Ball-on-disk configuration used in tribological characterization.

$$h = R(l - \cos \alpha) \qquad (03)$$

and

$$\alpha = \arcsin(l/2R)\ldots\ldots \qquad (04)$$

where l is the width of wear trace (μm), R is the ball radius (μm), h is the depth of trace (μm).

3. Results and discussion

3.1. Microstructural characterizations

3.1.1. Effect of milling time on grain size and grain size distribution

The particle size and morphology of the as-received and the high energy milled alumina powders are shown in Figs. 2 and 3 respectively. It can be observed in Fig. 2 that the as-received α-Al_2O_3 particles are irregular and angular shaped with a size distribution of 5–30 μm and were uniformly dispersed throughout the surface. It is observed from the SEM micrograph of as-received alumina (Fig. 2) that not only the grain size is smaller, but also the grain size distribution (visual inspection) is relatively small as well. It is obvious that the above mentioned powders were fine and had formed some agglomerates

The low mean average grain size can be attributed to the lower sintering temperature (1350 °C) applied for densification of the starting alumina powders. The grain size was measured using the linear intercept method. There is bimodal distribution of particle
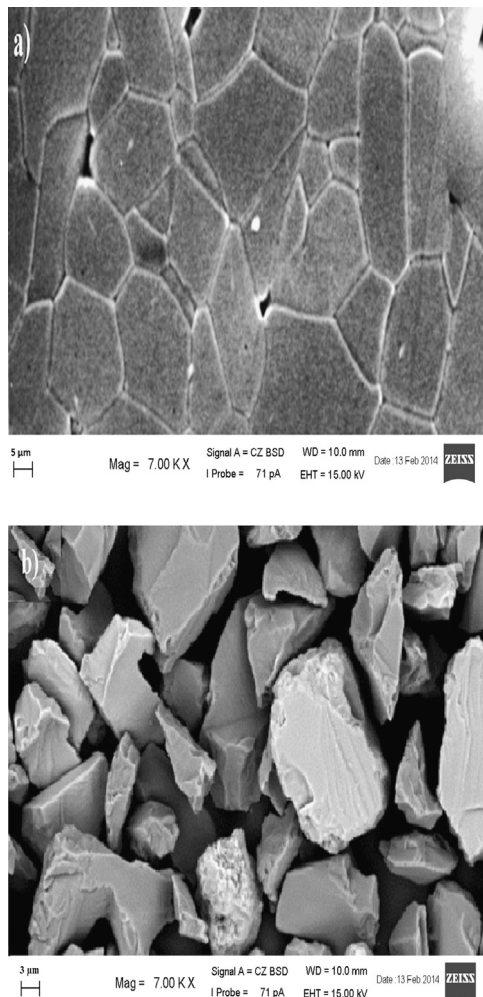

Fig. 2. SEM micrographic of as received materials (a) pressed and (b), as received particles powders alumina alpha.

sizes. The as-received powder had 90 vol% of the particles with size less than 30 μm and 10 vol% of the particles with size less than 10 μm.

SEM images of powder particles after the high energy milling at different milling times are shown in Fig. 3. From these SEM images, it is obvious that the above mentioned powders were fine and had formed some agglomerates. When powders are mechanically milled, the energy of milling deforms the particles and gets flattened by a micro-forging process. In these images elongated, irregular grains with sharp edges were present. In the samples milled for 1, 8, and 16 h a few large grains and an increase in the amount of fine grains was observed. In the sample milled for 24 h cluster of agglomerates appeared. With increasing milling time the powder particle size decreased due to the predominance of fracturing of powder particles over the cold welding process. Moreover, the flake morphology changed to equeiaxed morphology with increasing milling time. At longer milling times the powder particles were more uniform in size compared to early stages of milling (*Ceramic powders have the tendency to agglomerate due to the attractive intra-particle Van der Waals forces*). The larger particles at longer milling times, appears to be an agglomeration of many particles.

After 1 h of milling time the powder particles had flake morphology. With increasing milling time the energy of milling deforms the particles and they acquire flattened shapes by a micro-forging process and the powder particle size reduces to 1–5 μm due to the predominance of fracturing of powder particles over the cold welding process. It can also be observed that the flake morphology changed to equiaxed morphology with increasing milling time. At longer milling time (24 h) the powder particles were more uniform in size compared to that of shorter milling times. The larger particles observed after longer milling times may be due to the agglomeration of many particles. It is observed that the milled powder consists of 50 vol% particles with size smaller than 50 nm and 50 vol% particles with size smaller than 10 nm. It is, however, important to note that while the particles less than 50 nm could be clearly seen; those less than 10 nm have agglomerated. The extent of agglomeration is quite significant for the 50 nm size particles.

3.1.2. Effect of milling time on the morphology of α-Al_2O_3

The XRD patterns (Fig. 4) of alumina powder mixture at different milling times show that they consist only of α-Al_2O_3. The corresponding diffractograms to the lattice planes (012), (104), (110), (006), (113), (116), (211), (122), (214), (125), (208), (300), (101) and (220) are indicated.

As can be seen, the position of the maximum peaks in the patterns of alumina as function of milling time is similar but with increasing milling times the intensity of diffraction peaks decreases and their width increases progressively as a result of the refinement of crystallite size and enhancement of lattice strain which is in agreement with the results obtained by Nicolaiset et al. [49]. With increasing milling time the brittle particles (Al_2O_3) are uniformly dispersed.

After 24 h of milling, we observed that the reflection peaks corresponding to (006), (024), (101) and (113) totally disappear and the other peaks slightly shift towards lower angles.

The evolution of the average crystallite size $\{D\}$ and the average internal mean strain $\{\varepsilon\}$ of the α-Al_2O_3 phase in milled system as a function of milling time are presented in Fig. 5. It is predicted that if the milling process continues, the grains will become finer until they reach a critical value. The rational reason for this prediction is that mechanical milling is the result of the competition between cold fusions and breaking procedures of components that cause the fineness and the activation of particles. At the critical point, the
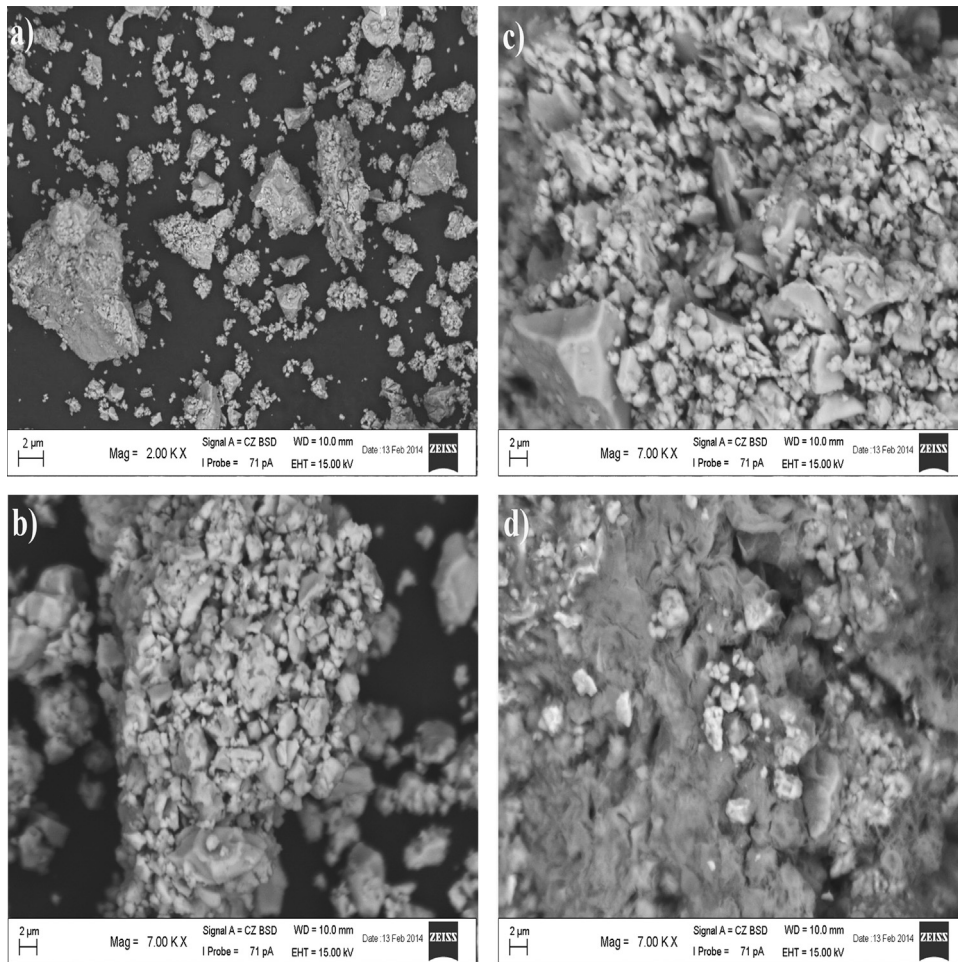
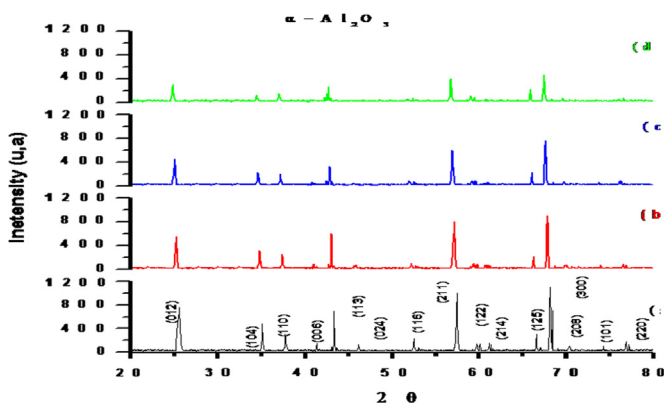**Fig. 3.** SEM images of powder particles after (a) 1 h, (b) 8 h, (c) 16 h and (d) 24 h of milling times.

Fig. 4. XRD patterns of α-Al$_2$O$_3$ powder milled at different milling times after (a) 1 h, (b) 8 h, (c) 16 h and (d) 24 h of milling times. The peak height decrease and broadening with increased milling time is evident.

Fig. 5. Average crystallite size {D} (nm) and mean internal microstrain {ε} (%) of α-alumina powder mixture versus milling time.

speed of fusion and breaking will be balanced and the particles will no longer be reduced in size [50,51].

As can be seen in Fig. 5, the crystallite size gradually decreased with increasing milling time, which is accompanied by an increase of the average strain rate {ε}. Similar dependencies of {D} and {ε} parameters on milling time were reported by many authors. The size of the crystallite and the rate of the internal strain of the un-milled powder mixture are 48 nm and 0.1%, respectively, and then decreases by almost half; i.e. 24.92 nm after 16 h to reach 20.72 nm after 24 h. Whereas the mean internal strain values
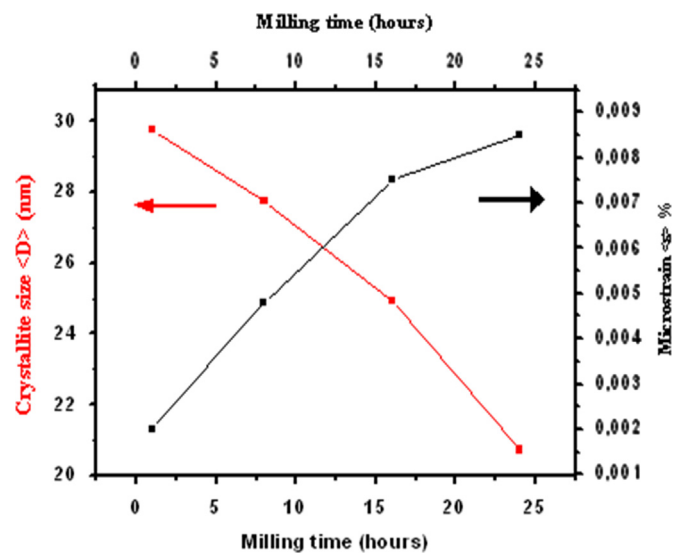
increases from 0.2% to 0.85%, respectively. The above results and observations can be attributed to the particle size refinement up to the nanometer scale followed by an increase in the strains induced at the internal level (alternate phenomena of breaking a weld).

A significant increase in the lattice parameters *a* and *c* is clearly observed in Fig. 6 after a milling time of 1 h. However as the milling time is increased to 24 h only the alpha alumina exists, and hence the relative increase in the lattice parameter is not as large as compared to the previous stages. As clearly observed in Fig. 6 the lattice parameter *a* increases with increasing of the milling time, from 0.475 nm after 1 h of milling to 0.479 nm after 24 h of milling, this represents an approximate cell volume expansion of 2.2% for the lattice parameter *a*, the lattice parameter *c* also increases with increasing of the milling time from 1.298 nm after 1 h of milling to 1.299 after 24 h milling which represents a cell volume expansion of approximately 2.4%. This increase is translated on XRD patterns (Fig. 3) by a shift of the peaks to smaller 2θ angles.

The same type of variation of the lattice parameter was also observed by some other authors as reported in the literature [52], which confirms the results obtained in this study. Generally, the increase of the cell parameters with the milling time arises mainly from two phenomena: (1) formation of the pound by mechanical milling, (2) the introduction of first order constraints during the

milling process which act on a macroscopic scale by modifying the cell parameters of the materials [52].

3.1.3. Effect of milling time on microhardness

The load-penetration depth curves obtained from nanoindentation test of nanostructured α-Al_2O_3 after different milling times (1, 8, 16 and 24 h) are shown in Fig. 7. The difference in hardness of the materials is apparent from the difference in the peak depth. Curves illustrate that the microhardness increased as a function of the milling time. The highest value, 2036 HV, was obtained after 24 h and the lowest value, 1942 HV, was obtained after 1 h milling time. It is noteworthy to point out that the reduction in the average crystallite size could also have a partial contribution in the resultant composite hardness due to grain refinement strengthening mechanism.

3.2. Tribological behavior

3.2.1. Effect of milling time on friction coefficient

Typical plots corresponding to the friction coefficients registered for different normal loads of 3, 6 and 10 N at a sliding velocity of 25 mm s^{-1} of nanocomposite α-Al_2O_3 milled for different times (1, 6, 16, and 24 h) are shown in Fig. 8.

As shown in the Fig. 8, the friction coefficient increases rapidly throughout the first meters of sliding and subsequently decreases. After this initial stage, the variations in the curves become smaller and the friction coefficient slightly increases during the remaining testing time. This behavior can be attributed to a polishing process during the wear test, establishing a smooth wear track surface, by plowing away the surface asperities or roughness irregularities.

As long as the wear test advances, wear tracks become smother and friction coefficients reach a steady state. It should be noted in Fig. 8(a) at 3 N at 1 h the samples exhibits much more fluctuations. More fluctuations can be due to extensive roughness of this sample. Additionally, with increasing hardness of the surface by increasing milling time (Fig. 7), the actual area of contact decreases; consequently, the COF values decrease.

It is obvious in Fig. 8 that, the friction coefficient showed a downward trend with the increase of the milling time, and was lower for higher applied load for all the tested samples. At 24 h of
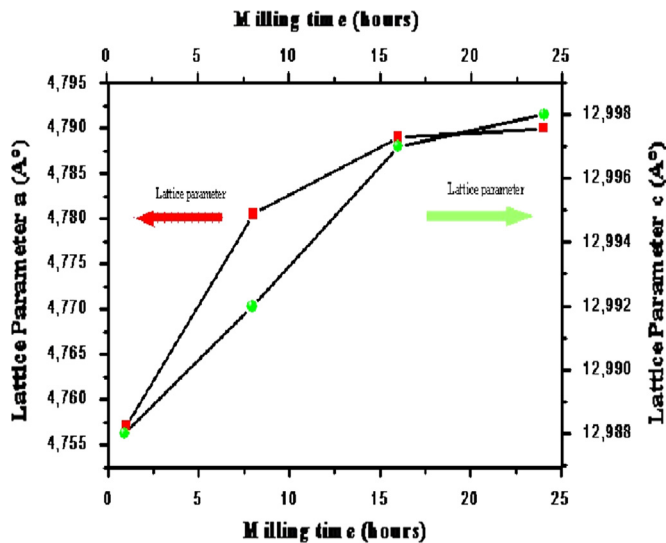

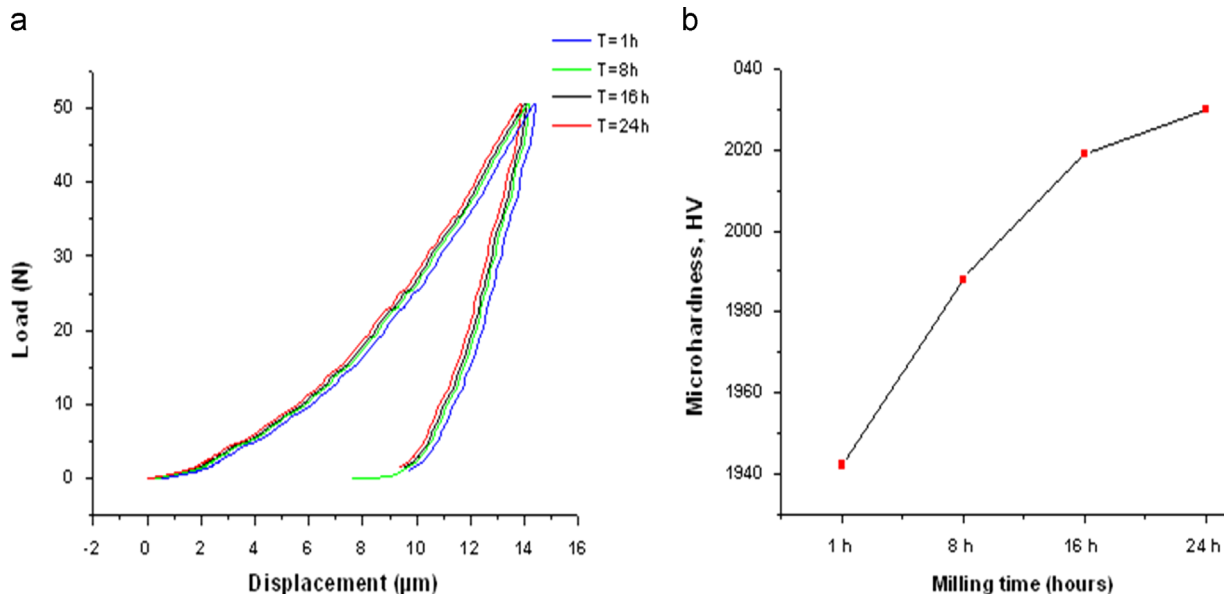**Fig. 6.** Lattice parameters {*a*} and {*c*} (Å) versus milling time for alpha alumina.

Fig. 7. (a) Load versus penetration depth (*P–h*) curve obtained from a nanoindentation test. (b) Hardness Vickers values versus milling time.
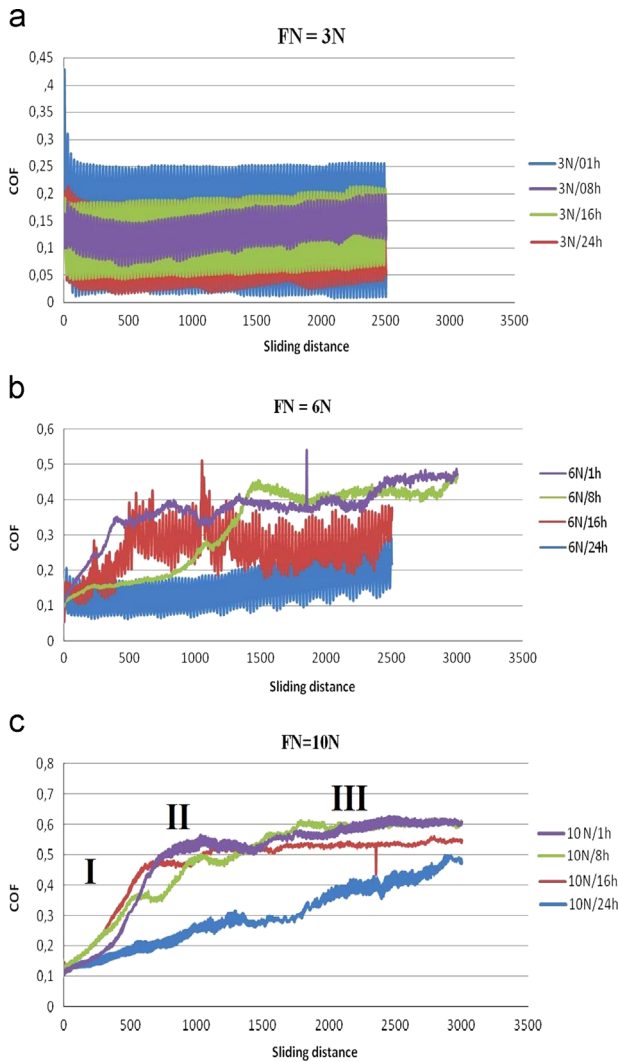
a

FN = 3N

b

FN = 6N

c

FN=10N

Fig. 8. Friction coefficient of milled alumina versus sliding distance: (a) Fn=3 N, (b) Fn=6 N and (c) Fn=10 N.

milling times the alumina exhibited the smallest and at 1 h the highest friction coefficient.

As can be seen in Fig. 9, the average mean values of the COF for samples at a normal load of 3 N is in the range of 0.112–0.133, while it varies between 0.15 and 0.4 for samples at 6 N, and 0.47–0.55 at 10 N with varying milling times of 24 to 1 h respectively.

It can be observed that with an increase in the normal load, the friction coefficient increases. This is because of an increase in the true contact area upon an increase in the normal load which leads to an increase in the friction coefficient.

3.2.2. Effect of milling time on wear rate

It can be observed from Fig. 10 that the wear rate of nanometric Al_2O_3 ceramics increases with an increase in load when the milling time was fixed. When the load was fixed, the wear rate tends to decrease with the increasing milling time. When the load was less than or equal to 6 N, the wear rate varied within the range of 1.30×10^{-3} to 11.57×10^{-3} μm^3 N μm^{-1}; whereas, when the load was higher than 6 N, the wear rate varied within the range of 11.13×10^{-3}–17.66×10^{-3} μm^3/N μm indicating that the wear was intensified. The wear rate was higher at lower milling time and lower at higher time.

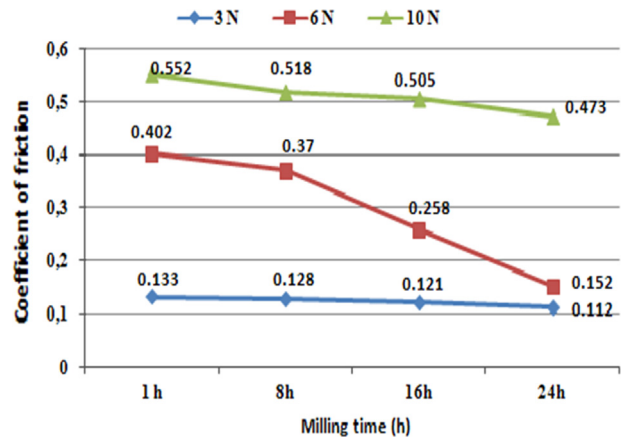**Fig. 9.** Mean friction coefficien of α-Al_2O_3 under different milling time.

a

b

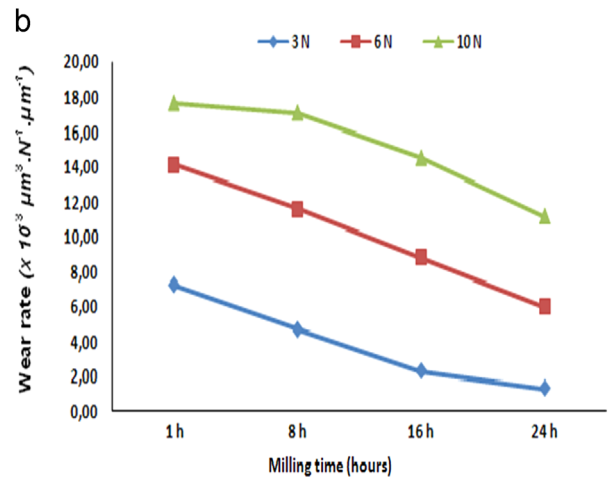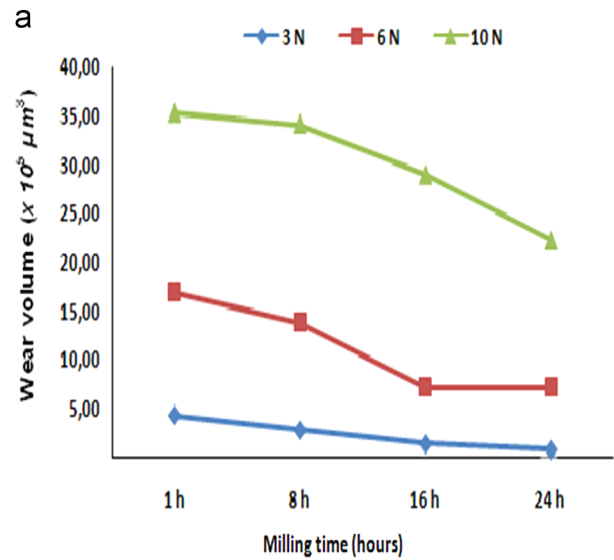**Fig. 10.** Evolution of: (a) Wear volume ($\times 10^5$ μm^3), (b) Wear rate ($\times 10^{-3}$ μm^3 N^{-1} μm^{-1}) of α-Al_2O_3 under different milling time.

It seems that the applied load and milling time have greater influence on the wear rates for the HIPed alumina with higher hardness and submicron grain size. All estimations made, range from 10^{-2} to 10^{-3} (μm^3/N μm) which means that there is a difference of about 1 order of magnitude between the lowest and the highest wear rates calculated.

The results confirm that the friction and wear resistance of the nanostructured α-Al$_2$O$_3$ not only depend on the applied load, but also depends on their milling time. As can be seen from Figs. 9 and 10, the samples milled for 24 h and tested at a normal load of 3 N exhibited lower friction and wear rates and better wear resistance. The higher wear resistance of nanostructured alpha alumina milled at 24 h can be atributed to its good mechanical propreties, higher values of hardness, lower crystallite and grain size.

The wear morphology of the worn surfaces after 3000 m of dry sliding wear was examined by SEM. Fig. 11(a–c) illustrate the typical α-Al$_2$O$_3$ alloy milled for 24 h, after the wear tests performed at normal loads of 3, 6 and 10 N respectively. It can be observed from the SEM micrographs, that an increase in the normal load, results in a significant build up of the material on the inner and outer periphery of the wear track. Moreover, an increase in the normal load resulted in wider grooves as well.

A significant surface damage with smeared, deformed appearance can be observed on the wear track. There are a lot of micro-cracks located on the worn surface indicating that brittle fracture took place. The wear track was mangled, and showed a brushing off of debris on the worn surface.

It can be observed from the SEM micrographs, that an increase in the normal load, results in a sinificant build up of the material on the inner and outer periphery of the wear track. Moreover, an increase in the normal load resulted in wider grooves as well. After comparison of the coarse particle size illustrated in Fig. 11(b–d),

the wide grooves in the worn surfaces of the fine particle size can be observed, this indicates that the main wear mechanism was abrasive wear. In the worn surface of the fine particle size. Lamination defect were observed and the weight loss was mostly caused by aghesive wear. Along the wear track both wear mechanisms, abrasive and adhesive wear, are vesible which occur at applied load. At a lower load, abrasion is the major wear mechanism while at higher loads adhesion is the main wear mechanism

Fig. 12(a–d) shows SEM micrographs corresponding to the worn surfaces of the milled alumina at 1, 8, 16 and 24 h respectively, after tribotesting at 10 N normal load. For these samples, a relatively smooth wear track is observed. Moreover, small sized wear debris particles are also observed which probably may have been removed from the material by plastic deformation. As indicated earlier, the higher wear resistance of nanostructured alpha alumina milled at 24 h can be atributed to its higher values of hardness. The ceramic microstructure also influences the material's properties, and with that, indirectly the tribological properties as well. The grain size (and distribution) and porosity of a sintered ceramic body directly influences some of the material properties like thermal shock resistance and bending strength.

The relationship between hardness and alumina grain size follows a Hall–Petch-type equation, which implies an increasing hardness with decreasing grain size [53]. Alumina with the smallest grain size shows the lowest wear rate, as expected.
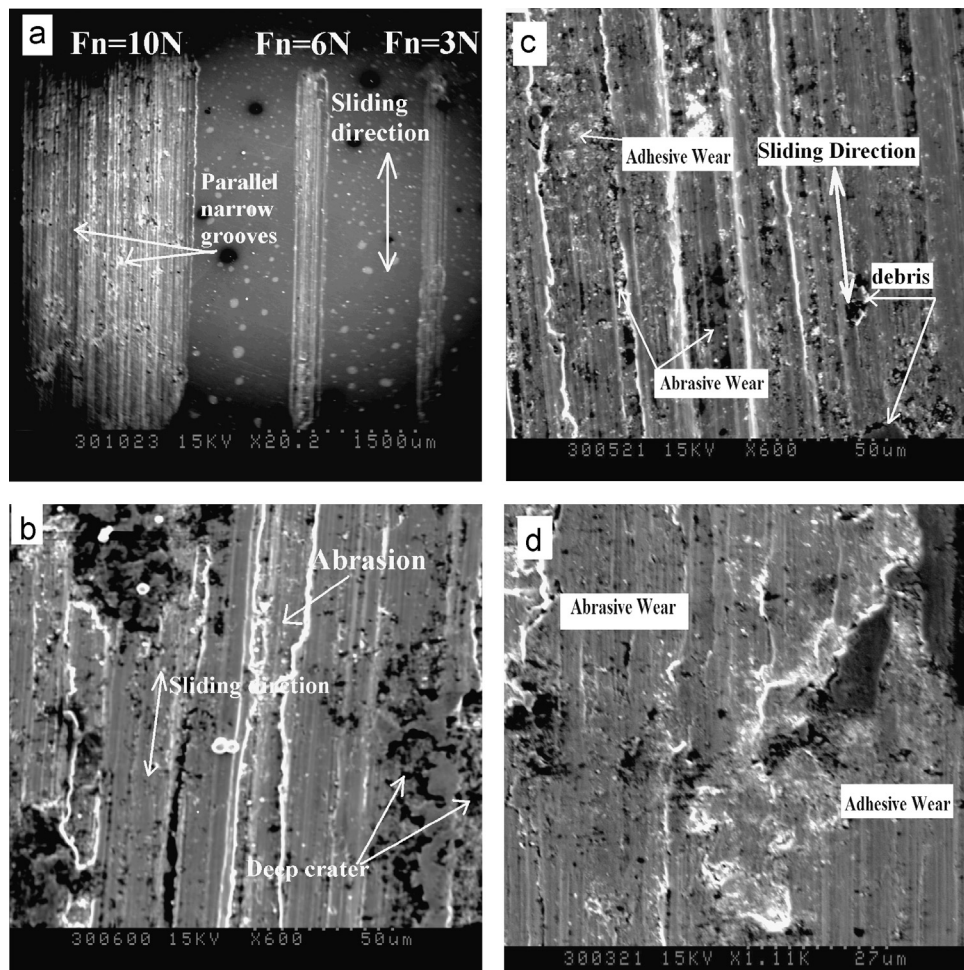

Fig. 11. SEM images of the worn surfaces of α-alumina specimens worn surface and particles sizes (b) 3 N, (c) 6 N and (d) 10 N, arrow indicates the direction of sliding.
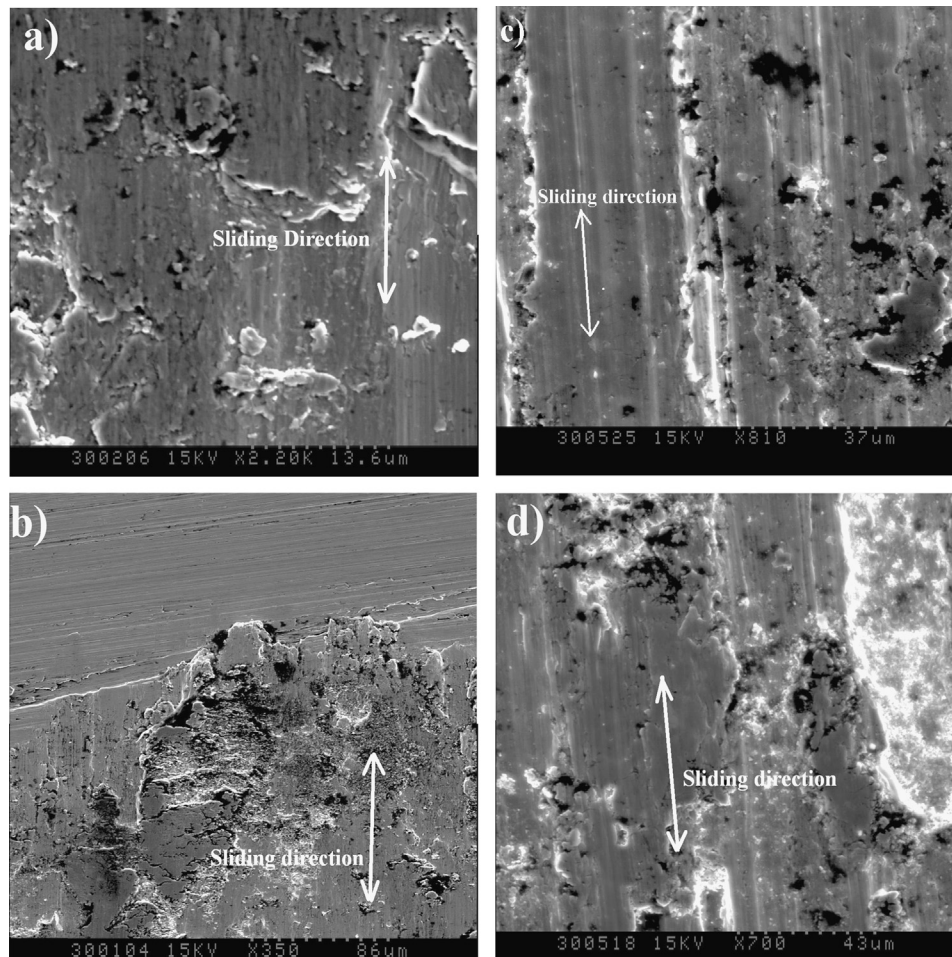
Fig. 12. SEM micrographs corresponding to the worn surfaces of the milled alumina at: (a) 1 h, (b) 8 h, (c) 16 h and (d) 24 h.

Hence, the improvement in the wear performance of nanostructured alpha alumina milled at 24 h can also be atributed its lower crystallite and grain size.

4. Conclusions

In this study, nanostructured powder of alumina was successfully prepared varying milling times using high energy planetary ball mill. Structural analysis highlighted the formation of nanostructured solution starting from 1 h of milling through 24 h of milling. The lattice parameters increased during milling and reached the value of $a = 0.497$ and $c = 12.998$. Whereas the crystallite size decreased up to 20 nm and rate of microstrain increased up to 0.85%. The morphology (changes of shape and size) of the milled powders was evaluated using a scanning electron microscopy (SEM). It was observed that the milling for a long periods of time favors the existance of particles of polyhedral shape with rounded corners.

HIPed nanostrucural α-Al_2O_3 composites were produced to further optimize its tribological behavior. Particular attention was paid to evaluate the effect of miling time and applied normal load on the friction and wear behaviors of these composites. Results showed that

- Milling of α-Al_2O_3 for longer times resulted in signicant improvement in relative density, hardness and wear resistance due to a decrease in the particle sizes.

- At constant applied normal loads, the wear rates decreased with increasing milling times which is attributed to the improved mechanical properties of the powders due to a reduction in their particle sizes.
- At the same milling times, an increase in the applied normal load increased the wear track width resulting in higher wear rates.
- The friction coefficient increased with increasing of the normal load, and also decreased significantly with higher milling time for all tested samples. The alumina milled at 24 h exibited the lowest friction coefficient, and at 1 h the highest under the identical test conditions.
- At 24 h milling time the alpha alumina showed the lowest wear rate, while at 1 h milling time the highest. The applied load, crystallite and grain size played and important role in controlling the wear rate. The higher wear resistance at 24 h miling time corresponded to it's good mechanichal and microstructural propreties.
- The governing wear mechanisms were found to be abrasion and delamination for nanostructured α-Al_2O_3 nanostructured.

According to our results, we obtained microstructures with final grain sizes lower than reported by other authors as well as high wear resistance, hardness and mechanical properties values compared with others investigations. It seems that this nanocomposite would be a good material for hip prostheses, which means a longer wear life of the components and thus providing the patient a better quality of life.

References

[1] Fellah M, Labaïz M, Assala O, Dekhil L, Zerniz N, Iost A. Tribological behavior of biomaterial for total hip prosthesis. Matér Tech 2014;102(6-7):601.

[2] Fellah M, Labaiz M, Assala O, Dekhiet L, Taleb A, rezzag H. Tribological behavior of Ti-6Al-4V and Ti-6Al-7Nb Alloys for Total Hip Prosthesis. Advances in Tribology 2014;2014:451387-1–13.

[3] Mc Kellop H, Clarke IC, Markolf KL. Friction and wear properties of polymer, metal, and ceramic prosthetic joint materials evaluated on a multichannels screening device. J Biomed Mater Res 1981;15(5):619–53.

[4] Mc Kellop H, Lu B, Benya P. Friction lubrication and wear of cobalt–chromium, alumina and zirconia hip prostheses compared on a joint simulator. In: Proceedings of the ORS 38th annual meeting. Washington, DC; 1992 p. 16–20.

[5] Fellah M, Labaïz M, Assala O, Iost A, Dekhil L. Tribological behavior of AISI 316L stainless steel for biomedical applications. Tribology-Marerials Surfaces & interfaces 2013;7(03):135–49.

[6] Oonishi H, Igaki H, Takayama Y. Comparisons of wear of UHMWPE sliding against metal and alumina in total hip prosthesis. Bioceramics 1989;1 272–27.

[7] Fellah M, Labaïz M, Assala O, Iost A. Tribological behavior of friction couple: metal/ceramic (used for head of total hip replacement). In: Narayan R, Colombo P, Kirihara S, Widjaja S, editors. Advances in Bioceramics and Porous Ceramics VI, VI. Hoboken, NJ, USA: John Wiley & Sons, Inc.; 2014. p. 45–57. http://dx.doi.org/10.1002/9781118807811.ch4.

[8] Griss P, Heimke G. Five years experience with ceramic–metal composite hip en do prostheses. I. Clinical evaluation. Arch Orthop Trauma Surg 1981;98:157–64.

[9] Shimizu K, Oka M, Kumar P. Time-dependent changes in the mechanical properties of zirconia ceramic. J Biomed Mater Res 1993;27:729–34.

[10] Cales B. Zirconia as a sliding material. Clin Orthop Relat Res 2000;379:94–112.

[11] Slonaker M, Goswami T. Review of wear mechanisms in hip implants: paper II–ceramics IG004712. Mater Des 2004;25:395–405.

[12] Sharma A, Komistek RD, Ranawat CS, Dennis DA, Mahfouz MR. In vivo contact pressures in total knee arthroplasty. J Arthroplast 2007;22(3):404–16.

[13] Komistek RD, Kane TR, Mahfouz MR, Ochoa JA, Dennis DA. Knee mechanics: a review of past and present techniques to determine in vivo loads. J Biomech 2005;38(2):215–28.

[14] Fellah M, Assala O, Labaïz M, Dekhil L, Iost A. Friction and wear behavior of Ti–6Al–7Nb biomaterial alloy. J Biomater Nanobiotechnol 2013;4:374–84.

[15] Dennis DA, Komistek RD. Kinematics of mobile-bearing total knee arthroplasty. Instr Course Lect 2005;54:207–20.

[16] Hausselle J, Drapier S, Geringer J. Flaws growth modelling in zirconia acetabular cups of hip prostheses under microseparation. Mec Ind 2008;9:153–8.

[17] Stewart TD, Tipper JL, Insley G. Severe wear and fracture of zirconia heads against alumina inserts in hip simulator studies with microseparation. J Arthroplast 2003;18:726–34.

[18] De Aza AH, Chevalier J, Fantozzi G. Crack growth resistance of alumina, zirconia and zirconia toughened alumina ceramics for joint prostheses. Biomaterials 2002;23:937–45.

[19] Dennis DA, Komistek RD. Kinematics of mobile-bearing total knee arthroplasty. Instr Course Lect 2005;54:207–20.

[20] Komistek D, Mahfouz, Dennis. In vivo contact stresses for subjects implanted with metal-on-metal and ceramic-on-ceramic THAs. In: 55th ORS annual meeting, Las Vegas, NV Poster; 2009.

[21] Pavol Švec, Alena Brusilová, Jana Kozánková. Effect of microstructure and mechanical properties on wear resistance of silicon nitride ceramics. Materials Engineering. Materiálové inžinierstvo. - ISSN 1335-0803 2009;16(01):34–40.

[22] Estili Mehdi, Echeberria J, Vleugels J, Vanmeensel K, O leksandr B. Sintering in a graphite powder bed of alumina-toughened zirconia/carbon nanotube composites: a novel way to delay hydrothermal degradation. Ceram Int Part B 2015;41(3):4569–80.

[23] Xianglong H, Zuozhong L, Li F, Wei W, Jianfeng C. Co-precipitated synthesis of Al$_2$O$_3$–ZrO$_2$ composite ceramic nanopowders by precipitant and drying method regulation: a systematic study. Ceram Int Part A 2015;41(1):505–13.

[24] Martín MI, Rabanal ME, Gómez LS, Torralba JM, Milosevic O. Microstructural and morphological analysis of nanostructured alumina particles synthesized at low temperature via aerosol route. J Eur Ceram Soc 2008;28(13):2487–94.

[25] Ibrahim A, Hamid ZA, Aal AA. Investigation of nanostructured and conventional alumina–titania coatings prepared by air plasma spray process. Mater Sci Eng A 2010;52 766-38.

[26] Rodriguez J, Rico A, Otero E. Indentation properties of plasma sprayed Al2O3 13% TiO2 nanocoatings. Acta Mater 2009;57:3148–56.

[27] Jordan EH, Gell M, Sohn YH. Fabrication and evaluation of plasma sprayed nanostructured alumina titania coating with superior properties. Mater Sci Eng A 2001;301:809.

[28] Gell M, Jordhan EH, Sohn YH. Development and implementation of plasma sprayed nanostructured ceramic coating. Surf Coat Technol 2001;146:4854.

[29] Tian W, Wang Y, Yang Y. Three body abrasive wear characteristics of plasma sprayed conventional and nanostructured Al$_2$O$_3$ 13% TiO$_2$ coatings. Tribol Int 2010;43:876–81.

[30] Goberman D, Sohn YH, Shaw L. Microstructure development of Al$_2$O$_3$ 13 wt% TiO$_2$ plasma sprayed coating derived from nanocrystalline powders. Acta Mater 2002;50:114152.

[31] Wang X, Padture NP, Tanaka H. Wear-resistant ultrafine grained ceramics. Acta Mater 2005;53:2717.

[32] Lawn BR. Fracture of brittle solids. 2nd ed.. Cambridge (UK): Cambridge University Press; 1993.

[33] Xinhua L, Zeng Y, Lee SW. Characterization of alumina-3% titania coating prepared by plasma spraying of nanostructured powders. J Eur Ceram Soc 2004;24:62734.

[34] Cetegen BM, Semenov SY, Goberman D. Deposition of multi-layered alumina titania coatings by detonation waves. Scr Mater 2003;48:14838.

[35] Chantikul P, Bennison SJ, Lawn BR. Role of grain size in the strength and R-curve properties of alumina. J Am Ceram Soc 1990;73:241927.

[36] Padture NP, Bennison SJ, Chan HM. Flaw-tolerance and crack- resistance proper- ties of alumina aluminum titanate composites with tailored micro- structures. J Am Ceram Soc 1993;76:231220.

[37] Shaw LL, Goberman DR, Gell M. The dependency of Microstructure and properties of nanostructured coatings on plasma spray conditions. Surf Coat Technol 2000;130:18.

[38] Willmann G. Ceramic femoral head retrieval data. Clin Orthop Rel res 2000;379:22–8.

[39] Thakur PY, Ram MY, Dinesh PS. Mechanical Milling: a Top down Approach for the Synthesis of Nanomaterials and Nanocomposites. J Nanosci Nanotechnol 2012;2(3):22–48.

[40] Tjong SC, Haydn C. Nanocrystalline materials and coatings. Mater Sci Eng 2004;R 45:1–88.

[41] Raming TP. The synthesis of nano-nano dual phase ceramic composites. With ref.-with summaries in Dutch. Enschede: Universityof Twente; 2000 Thesis.

[42] Numan S, Sami SH, Zishan HK, Adnan M, Ameer A, Esam A, et al. High-energy ball milling technique for ZnO nanoparticles as antibacterial material. Int J Nanomed 2011;6:863–9.

[43] Zhang X, Wang H, Koch CC. Mechanical behaviour of bulk ultrafine-grained and nanocrystalline Zn. Rev Adv Mater Sci 2004;6:53–93.

[44] Geuzens E, Mullens S, Cooymans J, Luyten J, Lemoisson F, Sastry L. Synthesis and mechanical and tribological characterization of alumina–ttria stabilized zirconia (YSZ) nanocomposites with YSZ synthesized by means of an aqueous solution–gel method or a hydrothermal route. Ceram Int 2008;34(5):1315–25.

[45] Suryanarayana C. Mechanical alloying and milling 2001;45:1–184J Prog Mater Sci 2001;45:1–184.

[46] Hesham M, Elmkharram A. Mechanically processed alumina reinforced ultra-high molecular weight polyethylene (UHMWPE) Matrix composites. Thesis. Blacksburg, VA: Virginia Polytechnic Institute and State University; 2013.

[47] Fellah M, Assala O, Labaiz M. Comparative study on tribiological behavior of Ti–6Al–7Nb and SS AISI 316L alloys, for total hip prothesis. Hoboken, NJ, USA: John Wiley & Sons, Inc.; 2014. p. 237–46.

[48] Bocanegra-Bernal MH. Hot isostatic pressing (HIP) of α-Al$_2$O$_3$ submicron ceramics pressure less sintered at different temperatures: improvement in mechanical properties for use in total hip arthroplasty (THA). Int J Refract Met Hard Mater 2009;27:900–6.

[49] Nicolais L, Carotenuto G. Metal-polymer nanocomposite. INC. Italy: John Wiley & Sons; 2005. p. 145170.

[50] Razavi M, Rahimipour MR, Rajabi Zamani AH. Synthesis of nano crystalline TiC powder from impure Ti chips via mechanical alloying. J Alloy Compd 2000;436:142–5.

[51] Razavi M, Rahimipour MR, Mansoori R. Synthesis of TiC Al$_2$O$_3$ nano composite powder from impure Ti chips, Al and carbon black by mechanical alloying. J Alloy Compd 2008;450:463–7.

[52] Gastex L, Lebrun JL, Maeder G, Spraul JM. Détermination des contraintes résiduelles par diffraction des rayons X", no. 22. Publication Scientifique et technique ENSAM, Paris, p. 51–60.

[53] Hah SR, Fischer TE, Gruffel P, Carry C. Effect of grain boundary dopants and mean grain size on tribomechanical behavior of highly purified alpha—alumina in the mildregime. Wear 1995;181–183:165–77.